High electromechanical response in the non morphotropic phase boundary piezoelectric system $PbTiO_3$-$Bi(Zr_{1/2}Ni_{1/2})O_3$

Rishikesh Pandey,[1] Bastola Narayan,[1] Dipak Kumar Khatua,[1] Shekhar Tyagi,[2] Ali Mostaed,[3] Mulualem Abebe,[1] Vasant Sathe,[2] Ian M. Reaney,[3] and Rajeev Ranjan[1,*]

[1]*Department of Materials Engineering, Indian Institute of Science, Bangalore 560012, India*

[2]*UGC-DAE Consortium for Scientific Research, University Campus, Khandwa Road, Indore 452001, India*

[3]*Department of Materials Science and Engineering, University of Sheffield, Sheffield S13JD, United Kingdom*

(Received 8 December 2017; revised manuscript received 9 May 2018; published 27 June 2018)

There is a general perception that a large piezoelectric response in ferroelectric solid solutions requires a morphotropic/polymorphic phase boundary (MPB/PPB), i.e., a composition driven interferroelectric instability. This correlation has received theoretical support from models which emphasize field driven polarization rotation and/or interferroelectric transformations. Here, we show that the ferroelectric system $(1-x)PbTiO_3$-$(x)Bi(Zr_{1/2}Ni_{1/2})O_3$ (PT-BNZ), which shows d_{33} (∼400 pC/N) comparable to the conventional MPB/PPB systems, does not belong to this category. In the unpoled state the compositions of PT-BNZ showing large d_{33} exhibit a coexistence of tetragonal and cubiclike (CL) phases on the global length scale. A careful examination of the domain strucures and global structures (both in the unpoled and poled states) revealed that the CL phase has no symptom of average rhombohedral distortion even on the local scale. The CL phase is rather a manifestation of tetragonal regions of short coherence length. Poling increases the coherence length irreversibly which manifests as poling induced CL $\rightarrow$ $P4mm$ transformation on the global scale. PT-BNZ is therefore qualitatively different from the conventional MPB piezoelectrics. In the absence of the composition and temperature driven interferroelectric instability in this system, polarization rotation and interferroelectric transformation are no longer plausible mechanisms to explain the large electromechanical response. The large piezoelectricity is rather associated with the increased structural-polar heterogeneity due to domain miniaturization without the system undergoing a symmetry change. Our study proves that attainment of large piezoelectricity does not necessarily require interferroelectric instability (and hence morphotropic/polymorphic phase boundary) as a criterion.

DOI: 10.1103/PhysRevB.97.224109

I. INTRODUCTION

Ever since its discovery five decades ago, $Pb(Zr,Ti)O_3$ (PZT) -based alloys have been the most sought-after materials for pressure sensing, actuator, and transducer applications. Increased environmental concerns in the last decade and a half have stimulated the search for Pb-free alternatives. While this push has led to the discovery of new lead-free alloys exhibiting large piezoelectric response in $BaTiO_3$-based [1] and $K_{0.5}Na_{0.5}NbO_3$-based [2,3] systems, factors such as low Curie point (as in the case of $BaTiO_3$-based systems), and the difficulty in reproducing the desired phases (and hence properties) due to extreme sensitivity to slight changes in synthesis conditions [as in the case of $(K,Na)NbO_3$-based systems], are important hurdles regarding the commercial acceptability of these new lead-free materials. Also, the nonvertical nature of the morphotropic/polymorphic phase boundary (MPB/PPB) of these systems imparts a great deal of temperature sensitivity to piezoelectric properties which is not desirable from the device perspective. In this scenario it is worthwhile to explore other alternative systems including materials with reduced Pb content. Here, by low-lead piezoelectric systems we mean that the A site of the perovskite structure has a significant fraction of non-Pb cations, which can be contrasted with the all-lead piezoelectric systems such as $Pb(Zr_xTi_{1-x})O_3$ (PZT), $Pb(Mg_{1/3}Nb_{2/3})_{1-x}Ti_xO_3$ (PMN-PT), $Pb(Zn_{1/3}Nb_{2/3})_{1-x}Ti_xO_3$ (PZN-PT), and the like. Ferroelectric solid solutions with the general formula $PbTiO_3$-$Bi(M'M'')O_3$ (PT-B $M'M''$) can be attractive candidates in this regard as they usually exhibit a high Curie point, can be compositionally tailored to exhibit very good piezoelectric response, and are easy to make with reproducible properties [4–7].

Unlike the all-Pb piezoelectric systems where the end members such as $PbTiO_3$, $PbZrO_3$, $Pb(Mg_{1/3}Nb_{2/3})O_3$, $Pb(Zn_{1/3}Nb_{2/3})O_3$, etc., can crystallize as a perovskite phase when synthesized under ambient pressure conditions, the components $Bi(M'M'')O_3$ in PT-B$M'M''$ do not crystallize in the perovskite phase when synthesized at ambient pressure. The perovskite phase is rather formed only when the synthesis is carried out at high pressures (∼5–6 GPa) and high temperatures (∼1000 °C) [8–10]. However, for the sake of convenience, we may treat $Bi(M'M'')O_3$ as a virtual compound which can form a solid solution with other real perovskite compounds. The solubility of several B$M'M''$s is considerably high in $PbTiO_3$. Consequently, it can induce interesting changes in the crystal structure, ferroelectric, and piezoelectric properties of $PbTiO_3$ [11–20]. Examples include $Bi(Ni_{1/2}Ti_{1/2})O_3$-$PbTiO_3$ (BNT-PT) [11], $Bi(Mg_{1/2}Ti_{1/2})O_3$-$PbTiO_3$ (BMT-

*rajeev@iisc.ac.in

PT) [12,17,19], $Bi(Mg_{1/2}Zr_{1/2})O_3$-$PbTiO_3$ (BMZ-PT) [13,17,19], $Bi(Zn_{1/2}Ti_{1/2})O_3$-$PbTiO_3$ (BZT-PT) [14,18,19], $Bi(Zn_{1/2}Zr_{1/2})O_3$-$PbTiO_3$ (BZZ-PT) [14,19], $Bi(Zn_{1/2}Sn_{1/2})O_3$-$PbTiO_3$ [14], $Bi(Zn_{3/4}W_{1/4})O_3$-$PbTiO_3$ [15,18], $Bi(Mg_{3/4}W_{1/4})O_3$-$PbTiO_3$ (BMW-PT) [16], $Bi(Ni_{2/3}Nb_{1/3})O_3$-$PbTiO_3$ [20], etc. From the structural standpoint, depending on how they influence the tetragonality ($c/a = 1.06$) of $PbTiO_3$, the different PT-B $M'M''$ systems can be categorized into three groups: (i) those which increase the tetragonality such as $Bi(Zn_{1/2}Ti_{1/2})O_3$ and $Bi(Zn_{3/4}W_{1/4})O_3$ [14,15], (ii) those which do not affect the tetragonality such as $Bi(Zn_{1/2}Zr_{1/2})O_3$ and $Bi(Zn_{1/2}Sn_{1/2})O_3$ [14], and (iii) the majority which decrease the tetragonality of $PbTiO_3$. First principles calculations by Grinberg and Rappe [19] have shown that the overall polarization and tetragonality of PT-B $M'M''$ depends on the coupling between the off-centered displacement of ions on the A site (comprising of Pb and Bi ions) and those on the B site. While Bi substituting the Pb site in $PbTiO_3$ invariably enhances the ferroelectric distortion, the overall polarization and the tetragonal distortion of the alloy is determined by the type of elements M' and M'' replacing Ti on the B site [19].

Among the Bi/Pb-based solid solutions reported in the past, $PbTiO_3$-$BiScO_3$ (PT-BS) ($d_{33} \sim 450$ pC/N) [4,21] and $PbTiO_3$-$Bi(Ni_{1/2}Hf_{1/2})O_3$ ($d_{33} \sim 446$ pC/N) [7] have shown considerably high d_{33}. However, both Sc_2O_3 and HfO_2 are costly, which makes them unattractive for mass production and commercial application. Recently, the solid solution $(1-x)PbTiO_3$-$(x)Bi(Ni_{1/2}Zr_{1/2})O_3$ [$(1-x)$PT-(x)BNZ] was reported to show high d_{33}(~ 400 pC/N) [6]. The absence of costly elements makes it very attractive among the low-Pb category of piezoelectric materials. X-ray diffraction studies of PT-BNZ in the past have revealed that the compositions exhibiting large d_{33} exhibit a coexistence of tetragonal and cubiclike (CL) phases [11–13,17]. In analogy with the conventional MPB piezoelectric systems such as PZT, PMN-PT, etc., which show large piezoelectric response in the tetragonal and rhombohedral two-phase state [22,23], some groups have argued that the CL phase in PT-BNZ is also likely to be rhombohedral [6,11–13]. They attribute the CL appearance to very small rhombohedral distortion which cannot be detected due to limited resolution of the diffractometers. It may be noted that a similar CL phase has also been reported in other well-known ferroelectric systems such as $Na_{1/2}Bi_{1/2}TiO_3$-$BaTiO_3$ [24,25] and $Na_{1/2}Bi_{1/2}TiO_3$-$K_{1/2}Bi_{1/2}TiO_3$ [26].

The understanding of the nature of the CL phase is of great significance since it has great implication for our understanding of the mechanism(s) associated with the large piezoelectric response of this system. The two prominent mechanisms often invoked to explain large piezoelectricity in conventional MPB systems are (i) polarization rotation, which relates enhanced piezoelectric response to the ease of polarization rotation inside the unit cell [27–31], and (ii) enhanced mobility of the domain walls [32–35]. Some reports in the recent past have attributed field driven structural transformations as the dominant contributing mechanism to the large electromechanical response of MPB piezoelectrics [21,36–38]. Both field driven polarization rotation and interferroelectric transformation mechanisms rely on the system's proneness to exhibit composition/temperature induced interferroelectric instability—a hallmark of all MPB/PPB systems. If, as argued by some groups, the CL phase of PT-BNZ is rhombohedral, then the large electromechanical response of PT-BNZ can be rationalized in the framework of the mechanisms/theories developed for the MPB systems. If not, then we cannot invoke these as plausible mechanisms. Evidently, the clue for the understanding of the dominant mechanism contributing to the large piezoelectric response in PT-BNZ lies in resolving the symmetry of the CL phase. With this as the primary motivation, we carried out a comprehensive investigation of PT-BNZ using a variety of complementary experimental techniques involving electric-field- and temperature-dependent x-ray diffraction (XRD), transmission electron microscopy, Raman spectroscopy, dielectric, and piezoelectric measurements. We confirmed that the CL phase is not rhombohedral or its low-symmetry distortion. It is rather a manifestation of tetragonal regions of small coherence length. Thus what appears as two phase on the global scale is rather a coexistence of tetragonal regions of long and short coherence lengths. This rules out polarization rotation and/or interferroelectric transformation as possible mechanisms to explain the large electromechanical response in PT-BNZ. The large response in this system is therefore primarily associated with processes involving motion of the tetragonal domain walls.

II. EXPERIMENTAL DETAILS

Solid solutions of $(1-x)$PT-xBNZ were synthesized via the conventional solid-state ceramic route. High-purity analytical reagents (AR) grade Bi_2O_3 (99%), PbO (99.9%), NiO (99%), ZrO_2 (99.99%), and TiO_2 (99.8%) chemicals from Alfa Aesar were wet milled according to stoichiometric proportions in an agate jar with agate balls for 6 h using a planetary ball mill (Fritsch P5). The thoroughly mixed powder was calcined at 850 °C for 6 h. The calcined powder was mixed with 2 wt% polyvinyl alcohol-water solution and pressed into the form of disks of 15 mm diameter by using a uniaxial die at 8 tons. Sintering of the pellets was carried out between 1100 °C and 1150 °C for 3 h in a closed alumina crucible. Calcined powder of the same composition was kept inside the crucible as sacrificial powder during sintering. For XRD measurements, sintered pellets were crushed into fine powder and annealed at 500 °C for 6 h to remove the strains introduced during crushing. XRD data were collected using a Rigaku (SmartLab, Japan) diffractometer with a Johansson monochromator in the incident beam to remove the Cu-$K\alpha_2$ radiation. Dielectric measurement was carried out using a Novocontrol (Alpha-A, USA) impedance analyzer. For electrical measurements the sintered pellets were electroded by coating with silver paste and cured at 100 °C for 1 h. The electroded pellets were poled at room temperature in silicone oil for 1 h by applying a dc-electric field of 30 kV/cm. The longitudinal piezoelectric coefficient (d_{33}) was measured by poling the pellets at room temperature for 1 h at a dc-electric field of ~30 kV/cm using piezotest PM-300. The strain loop and the polarization electric-field (P-E) hysteresis loop were measured with a Precision premier II loop tracer (Radiant Technologies). Raman data were collected in the backscattering geometry using a diode laser excitation source (473 nm) coupled to a Labram-HR800 micro-Raman spectrometer equipped with a 50× objective

with an appropriate edge filter and a Peltier-cooled charge-coupled device detector. A THMS-600 stage (Linkam, UK) was used for temperature variation. Structure refinement was carried out by FULLPROF software [39]. Transmission electron microscopy (TEM) examination of the samples were carried out using JEOL 2100 (LaB_6) operated at 200 keV. The TEM specimens from both poled and unpoled samples were prepared using the conventional method, i.e., mechanical grinding and polishing followed by ion milling to electron transparency using Gatan PIPS II. Initial ion milling was performed using 5-keV Ar^+ ions at liquid nitrogen temperature and then surface damage was minimized by final low-energy milling steps at 500 and 100 eV.

III. RESULTS

A. Critical composition range

Figure 1 shows the evolution of the pseudocubic $\{111\}_{pc}$, $\{200\}_{pc}$, and $\{220\}_{pc}$ Bragg profiles of $(1-x)$PT-xBNZ with composition (x) in the range $0.38 \leqslant x \leqslant 0.44$. The profile $\{111\}_{pc}$ remains a singlet for all compositions. Dramatic changes can be seen in the $\{200\}_{pc}$ and $\{220\}_{pc}$ profiles for $x > 0.38$. While the $\{200\}_{pc}$ is a doublet for all $x \leqslant 0.38$ confirming a tetragonal $P4mm$ structure, an additional peak appears, the intensity of which grows with x in the composition range $0.39 \leqslant x \leqslant 0.42$. For $x \geqslant 0.43$, all the peaks appear singlet suggesting a CL phase. Based on this visual inspection of the Bragg profiles, whole pattern fitting of the XRD data was carried out using the Rietveld method with tetragonal $(P4mm)$ + cubic $(Pm\text{-}3m)$ average structures. We may note that the choice of cubic $(Pm\text{-}3m)$ structure here is only a matter of convenience and does not represent the real structure, as will be evident in the subsequent sections. As shown in Fig. 1, this structural model fits the data very well. The refined structural parameters for $(1-x)$PT-xBNZ are listed in Table I. The refined isotropic displacement parameters (B_{iso}) of the A-site cations were, however, very large (~3.0 Å^2), both in the tetragonal and the CL phases. We refined the anisotropic thermal parameters (U) of the A-site cations in the tetragonal phase. For other atoms only the B_{iso} were refined. This resulted in an overall good fit between experimental and calculated patterns. A very large displacement parameter of the A-site cations has also been reported in Pb-based relaxor systems and is often attributed to the local positional disorder of the atoms [40–43]. We may note that although the compositions $x = 0.44$ and $x = 0.38$ appear as pure CL and tetragonal, respectively, the fit was improved when the second minor phase was included in the structural model. Figure 2(b) shows the composition dependence of the lattice parameters and tetragonal phase fraction. The tetragonal a parameter increases and the c parameter decreases with increasing x. The rate of change of the parameters can be seen to decrease noticeably for $x > 0.40$. This is more clearly revealed in the composition variation of the tetragonality (c/a), Fig. 2(b). Interestingly, the tetragonal phase fraction follows the same trend as the tetragonality [Fig. 2(b)], suggesting a correlation between the two.

B. Electromechanical response

Figure 2(c) shows compositional dependence of the longitudinal piezoelectric coefficient (d_{33}). The highest d_{33}(~385 pC/N) was obtained for $x = 0.41$. This value is close to ~ 400 pC/N, reported before for this system [6]. Even $x = 0.44$, the composition exhibiting almost pure CL phase (Fig. 1), shows d_{33} as high as 260 pC/N, confirming its structure to be noncubic (ferroelectric) on the local length scale. Figure 3(a) shows the variation of unipolar electrostrain with the electric field up to an applied field of 60 kV/cm. The composition $x = 0.41$ shows the maximum electrostrain of 0.42%. This corresponds to a large signal converse piezoelectric response (d^*_{33}) defined as S_{max}/E_{max}, ~ 700 pm/V, Fig. 3(c). The magnitude of the electrostrain at 60 kV/cm is higher than what has been reported for the MPB compositions

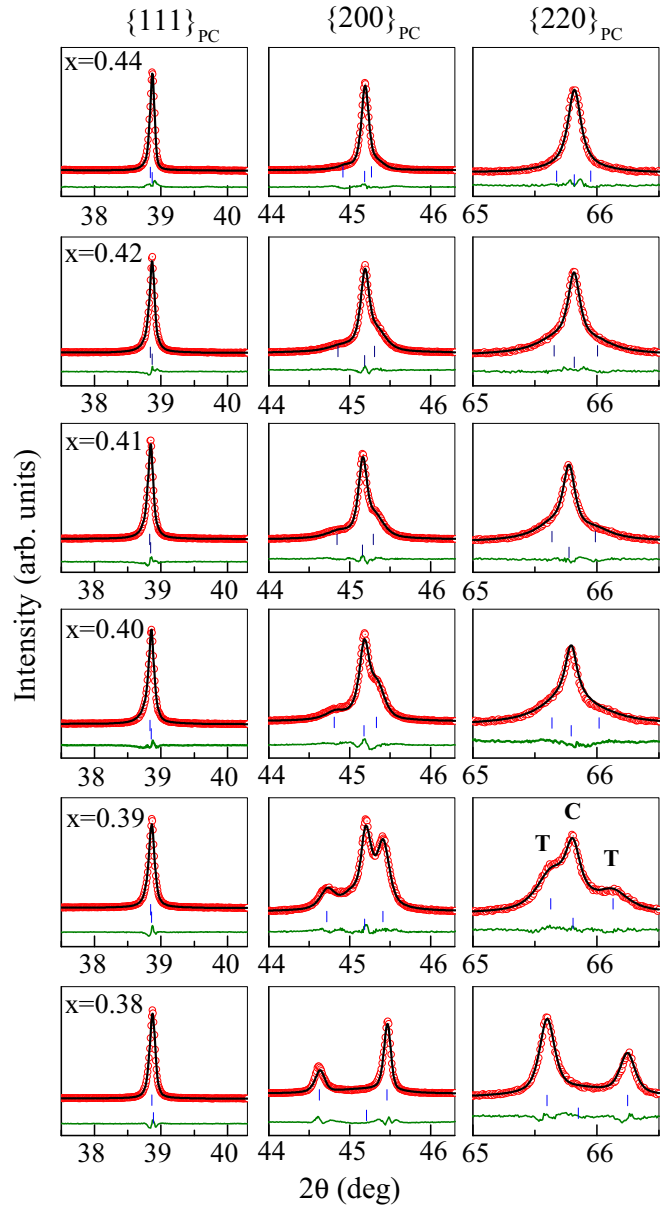

FIG. 1. Observed (circles), calculated (continuous line), and difference (continuous bottom line) Rietveld-fitted XRD profiles of $(1-x)$PT-(x)BNZ in the range $x = 0.38$–0.44 with a cubic $(Pm\text{-}3m)$ and tetragonal $(P4mm)$ phase coexistence model. The vertical tick marks show the position of Bragg peaks. T and C denote Bragg peaks corresponding to the tetragonal and the cubiclike phases, respectively.

TABLE I. Refined structural parameters and agreement factors for PT-BNZ with $x = 0.41$ using tetragonal $P4mm$ and cubic $Pm\text{-}3m$ space groups.

Composition	Ions	$P4mm$	$Pm\text{-}3m$
$x = 0.41$	Bi^{3+}/Pb^{2+}	$x = y = z = 0$, $U_{11} = U_{22} = 0.043(8)$ Å^2, $U_{33} = 0.014(1)$ Å^2	$B_{iso} = 3.0(0)$ Å^2
	$Ni^{2+}/Zr^{4+}/Ti^{4+}$	$x = y = 0.5$, $z = 0.5562(7)$, $B_{iso} = 0.1(5)$ Å^2	$B_{iso} = 0.2(1)$ Å^2
(Unpoled)	O_I^{2-}	$x = y = 0.5$, $z = 0.103(2)$, $B_{iso} = 1.0(0)$ Å^2	$B_{iso} = 0.6(1)$ Å^2
	O_{II}^{2-}	$x = 0.5, y = 0.0$, $z = 0.637(2)$, $B_{iso} = 0.8(1)$ Å^2	
		$a_T = 4.0003(1)$ Å, $c_T = 4.0388(2)$ Å, $\chi^2 = 1.54, R_{wp} = 8.16$	$a_C = 4.0122(3)$ Å
	Bi^{3+}/Pb^{2+}	$x = y = z = 0$, $U_{11} = U_{22} = 0.041(1)$ Å^2, $U_{33} = 0.028(1)$ Å^2	
(Poled)	$Ni^{2+}/Zr^{4+}/Ti^{4+}$	$x = y = 0.5$, $z = 0.5534(6)$, $B_{iso} = 0.4(1)$ Å^2	
	O_I^{2-}	$x = y = 0.5$, $z = 0.102(2)$, $B_{iso} = 1.0(0)$ Å^2	
	O_{II}^{2-}	$x = 0.5$, $y = 0.0$, $z = 0.629(2)$, $B_{iso} = 0.8(1)$ Å^2	
		$a_T = 3.9982(6)$ Å, $c_T = 4.04581(1)$ Å, $\chi^2 = 1.96$, $R_{wp} = 8.94$	

of PZT [45]. This composition ($x = 0.41$) also exhibits the smallest coercive field, Fig. 3(b). We succeeded in achieving electrostrain to $\sim 0.5\%$ on $x = 0.41$ when the electric-field amplitude was increased to 85 kV/cm, inset of Fig. 3(a). Given the fact that the electrostrain is sensitive to grain size, i.e., for any given composition, the electrostrain can be reduced by reducing the grain size of the specimen, we ensured that average grain size for all the compositions were nearly the same (4–5 microns), Fig. 4. This confirms that the trends in the properties shown in Figs. 2(c) and 3(a) are intrinsic (i.e., due to composition variation).

C. Poling driven irreversible structural changes on the global scale

Figure 5(a) shows the poling induced changes in the XRD patterns of $(1 - x)$PT-xBNZ. The XRD data were collected after (manual) crushing of the poled pellets to powder. This strategy allows us to get a preferred orientation free diffraction pattern with the individual grains retaining the irreversible structural changes brought about by the poling field [25,46,47]. The pseudocubic $\{111\}_{pc}$ and $\{200\}_{pc}$ XRD Bragg profiles of the poled PT-BNZ are shown in Fig. 5(a). In contrast to the unpoled state (Fig. 1), the poled specimens of all the compositions exhibit tetragonal structure. This is true even for the composition showing almost single phase CL ($x = 0.44$) in the unpoled state, Fig. 1. The refined structural parameters of poled $x = 0.41$ using tetragonal space group $P4mm$ are listed in Table I. Figure 5(b) shows the composition dependence of the tetragonality (c/a) of poled samples. For the sake of direct comparison, we also show in Fig. 5(b) the tetragonality of the tetragonal phase in their respective unpoled states. It is interesting to note that the tetragonality of the poled specimen is considerably larger than that in the unpoled specimen in the composition range $x \sim 0.40$–0.42. The difference is considerably reduced for $x = 0.39$, the composition exhibiting a larger fraction of the tetragonal phase, Fig. 2(b). This further confirms a correlation between the measured tetragonality and the fraction of the $P4mm$ present in the system. For $x = 0.39$, the system already has a majority of $P4mm$ in the unpoled

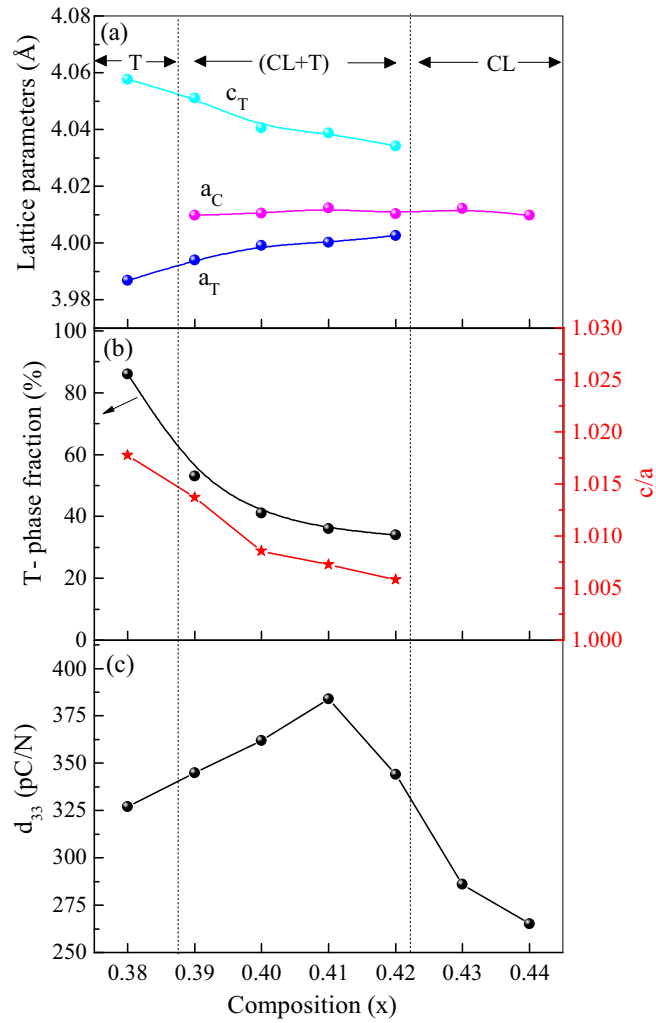

FIG. 2. (a) Composition dependence of the cubiclike lattice parameter (a_c), and tetragonal lattice parameters (c_T and a_T) of $(1 - x)$PT-xBNZ. (b) Composition dependence of tetragonal phase fraction and the tetragonality. (c) Composition-dependent longitudinal piezoelectric coefficient (d_{33}) for $(1 - x)$PT-xBNZ. The vertical dotted lines denote the two-phase ($P4mm$ + CL) region.

state. The scope of further increasing the coherehence length by the poling field is limited. On the other hand, $x = 0.44$ shows majority CL phase in the unpoled state. The poling induced CL $\rightarrow$ $P4mm$ is maximum here, and so is the maximum perceived change in the tetragonality after poling.

D. Confirmation of relaxor ferroelectricity

Figure 6 shows the temperature variation of the real (ε') and imaginary (ε'') part of the permittivity of $x = 0.41$. The broadness of the permittivity peak, and shifting of the permittivity maximum to higher temperature on increasing frequency, confirm relaxor ferroelectric behavior. Vogel-Fulcher analysis (inset Fig. 6) of the frequency dependence of the imaginary part of the permittivity (ε'') maximum temperature [48] suggests activation energy (E_a), relaxation time (τ_o), and the Vogel-Fulcher freezing temperature (T_f) as 3.38×10^{-3}eV, 2.08×10^{-7}s, and $\sim 257\,^{\circ}$C, respectively. Figures 7(a) and 7(b) compare the temperature variation of the dielectric permittivity of unpoled and poled specimens, respectively, of PT-BNZ ($x = 0.41$). A notable distinction is the occurrence of a small permittivity peak at $\sim 120\,^{\circ}$C in the poled sample [Fig. 7(b)], which is not visible in the unpoled specimen, Figure 7(a). We assign this temperature as the depolarization temperature (T_d) since the d_{33} of the specimen is abruptly reduced when the poled pellet was annealed at this temperature, Fig. 7(c). A significant departure from the Curie-Weiss behavior was also found below 470 °C [Fig. 7(d)], suggesting this to be the Burns temperature of this system below which polar nanoregions are expected to appear [49].

E. Depolarization and structural changes

To understand the nature of structural changes associated with the thermal depolarization on the global scale, we carried out high-temperature XRD measurement on poled PT-BNZ ($x = 0.41$). The structure of the poled specimen is tetragonal at room temperature, Fig. 8(a). On heating, separation between the two tetragonal peaks in the $\{200\}_{pc}$ profile decreases continuously. The onset of the CL peak can be seen at 130 °C. The CL and the tetragonal phases coexist up to 150 °C. The structure appears completely cubic at 200 °C, Fig. 8(a). This proves that the sharp drop in the d_{33} above 100 °C [Fig. 7(c)] is associated with the appearance of the CL phase. Figures 8(b)–8(d) show the temperature variation of the lattice parameters, unit-cell volume, and tetragonality. A weak anomaly in the temperature dependence of cell volume near the depolarization temperature ($\sim 150\,^{\circ}$C) can be seen.

F. Depolarization and lattice instability: Raman study

Figure 9(a) shows a Lorentzian fitted Raman spectrum of $x = 0.41$. Before fitting, the data were corrected with the Bose-Einstein factor. The Raman modes were assigned following earlier studies [50,51]. Due to instrumental limitations we did not consider peaks below 100 cm^{-1} for analysis. The first peak in our spectrum appears at $\sim$180 cm^{-1}, which is assigned as the A_1(1TO) mode. The other peaks are assigned as E(2TO) $\sim$ 227 cm^{-1}, (B_1 + E) $\sim$ 277 cm^{-1}, A_1(2TO) $\sim$ 320 cm^{-1}, E(3TO) $\sim$ 488 cm^{-1}, A_1(3TO) $\sim$ 585 cm^{-1}, E(3LO) $\sim$ 700 cm^{-1}, and

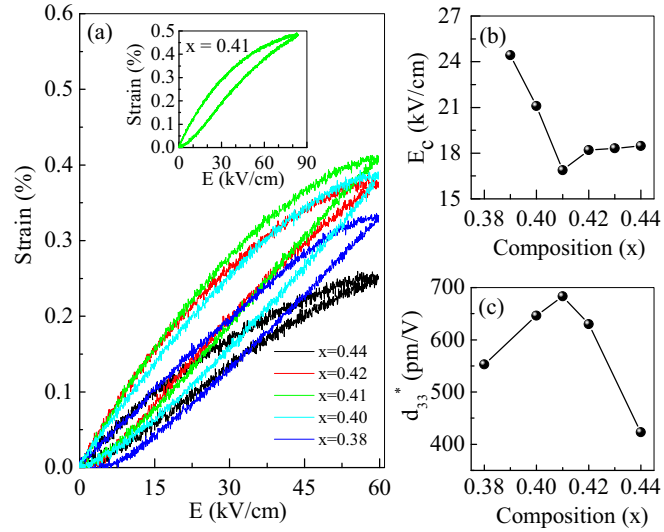

FIG. 3. (a) Electric-field (E) -dependent unipolar strain (%) of $(1-x)$PT-xBNZ. Inset shows the unipolar electrostrain of $x = 0.41$ for an applied field amplitude of 85 kV/cm. (b) Composition-dependent coercive field, and (c) large signal piezoelectric coefficient (d^*_{33}).

A_1(3LO) $\sim$ 760 cm^{-1}. With respect to the parent compound $PbTiO_3$, the A_1(1TO) is considerably hardened in our system (it increases by $\sim$ 28 cm^{-1}, i.e., from $\sim$ 152 cm^{-1} in $PbTiO_3$ to $\sim$ 180 cm^{-1}). A perusal of the literature suggests that this is a common feature of most Bi-substituted Pb-based perovskites. For example, the A_1(1TO) mode is reported at $\sim$ 185 cm^{-1} for 0.4$PbTiO_3$-0.6$BiFeO_3$ [18], at $\sim$ 172 cm^{-1} for 0.65$PbTiO_3$-0.35 $Bi(Zn_{1/2}Ti_{1/2})O_3$ [18], and $\sim$ 185 cm^{-1} in 0.66$PbTiO_3$-0.34 $BiScO_3$ [52]. The A_1(1TO) mode is associated with off-center polar displacement of A-site cations (Bi^{3+}/Pb^{2+}) with respect to BO_6 octahedra in $A-BO_3$ translational mode vibration [51].

Figure 9(b) compares the Raman spectra of the poled and unpoled specimens of $x = 0.41$ at room temperature. In contrast to the remarkable changes in the XRD pattern after poling [Fig. 5(a)], there are no such remarkable changes in the Raman spectra of the poled sample. Since Raman spectroscopy probes structural coherence on the local length scale, the nearly identical spectra of the CL (before poling) and tetragonal (after poling) phases suggest that the local structure of the tetragonal and the CL phases are nearly similar. On careful examination, however, we noted a slight decrease in the intensity of the mode at $\sim$ 320 cm^{-1} in the poled sample. We measured the Raman spectra of the poled specimen on first heating up to 400 °C, Fig. 10(a), and then during cooling. Since the specimen was heated well above the dielectric maximum temperature [$\sim$270 °C, Fig. 6(a)], the Raman spectra recorded during the cooling cycle can be regarded as those of the unpoled specimen. Figure 10(b) shows the intensity of the mode at $\sim$ 320 cm^{-1} during the heating and cooling runs. The poling induced loss in intensity of this mode [Fig. 10(b)], recovered during the cooling cycle below 150 °C [Fig. 10(d)], i.e., below the depolarization temperature. Another notable feature is the softening of the A_1(1TO) mode $\sim$ 180 cm^{-1} [Fig. 10(c)] on heating, and it is becoming invisible above 200 °C [Fig. 10(a)].

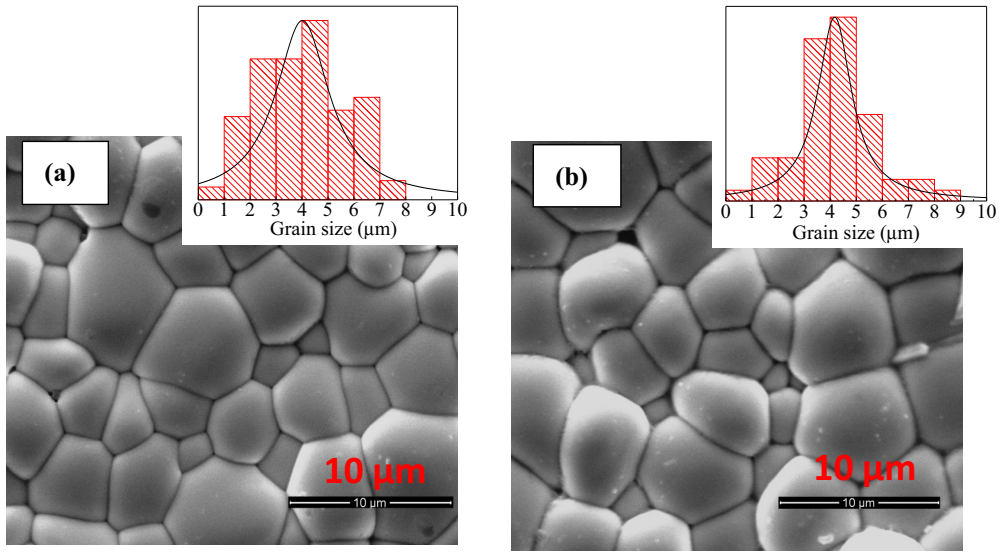

FIG. 4. SEM images of sintered pellets of $(1-x)$PT-xBNZ (a) $x = 0.41$ and (b) $x = 0.38$. The grain size distribution is shown by the histogram on the corresponding SEM image.

This confirms the role of lattice instability in the thermal depolarization of the system.

G. Local structure: TEM study

While XRD is a powerful technique to measure the average structure of the specimens (e.g., those measurements shown in Sec. II A), transmission electron microscopy offers the opportunity to study the structure of materials locally. For the TEM study we chose the composition $x = 0.42$ which exhibits a higher fraction of CL phase in the unpoled state as compared to $x = 0.41$ (the composition showing maximum d_{33}). We note, however, for samples close to the structural phase boundary electron beam–sample interaction induced changes in the domain structure over time during irradiation. All efforts were made to obtain representative images of the poled and unpoled domain structures before such modifications occurred. Figure 11(a) shows TEM data acquired from the poled sample with $x = 0.42$ close to a [100] direction of the perovskite cell (diffraction pattern is 4°–5° from the precise zone and inset). For simplicity all miller indices relate to the fundamental perovskite structure. The domain widths are ~0.1−0.2 μm, typical for Pb-based ferroelectrics. The domain walls have strong fringe contrast implying that they are inclined rather than perpendicular to the surface of the TEM sample. The top right-hand inset of Fig. 11 shows a region of the grain which

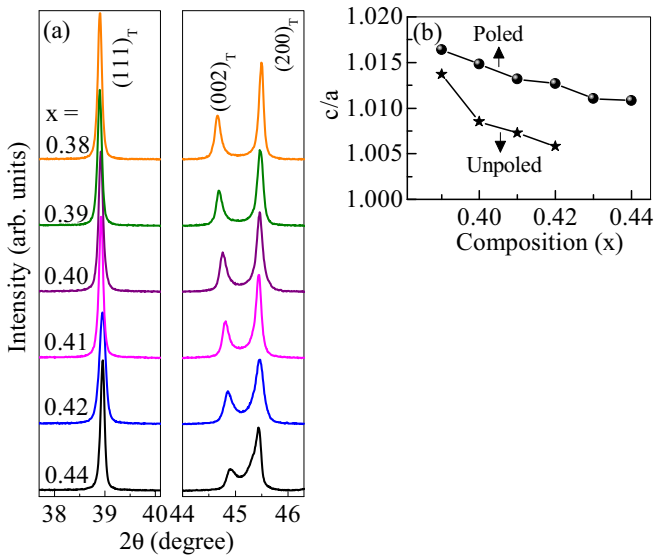

FIG. 5. (a) Pseudocubic $\{111\}_{pc}$ and $\{200\}_{pc}$ XRD Bragg profiles of poled $(1-x)$PT-xBNZ. The peaks are indexed with respect to the tetragonal $P4mm$ cell. (b) Composition dependence of the tetragonality of poled and unpoled $(1-x)$PT-xBNZ.

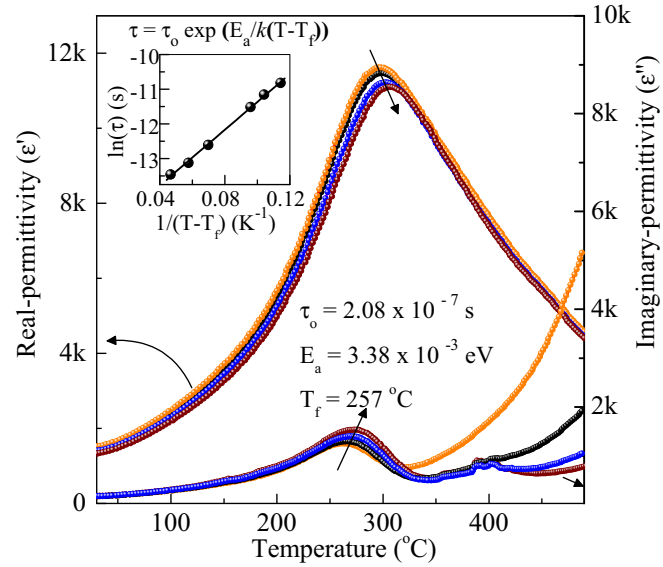

FIG. 6. Temperature dependence of the real and imaginary parts of the permittivity of PT-BNZ ($x = 0.41$) measured at 80, 100, 200, and 400 kHz. The arrows on the peaks show increasing frequency. Inset shows the Vogel-Fulcher fit.

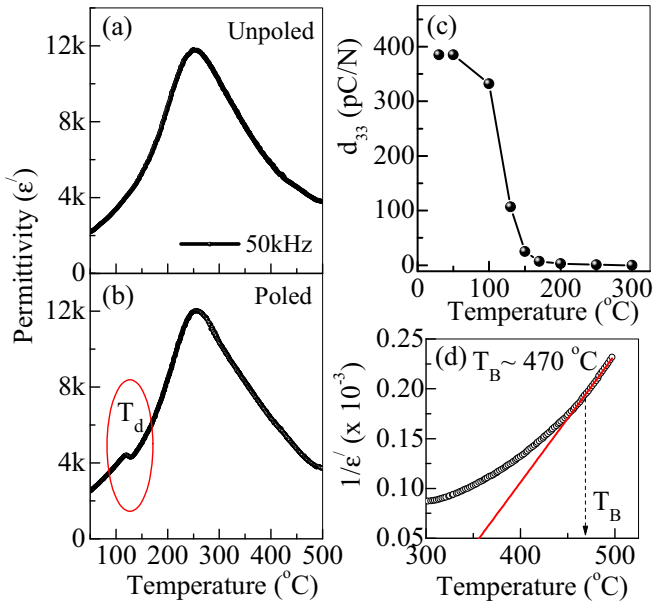

FIG. 7. Temperature dependence of the real part of permittivity: (a) unpoled, (b) poled PT-BNZ ($x = 0.41$) measured at 50 kHz. T_d corresponds to depolarization temperature. (c) Variation of d_{33} with annealing temperature. (d) $1/\varepsilon'$ vs T plot and Curie-Weiss fit of the real part of the permittivity of PT-BNZ, $x = 0.41$. T_B corresponds to Burns temperature.

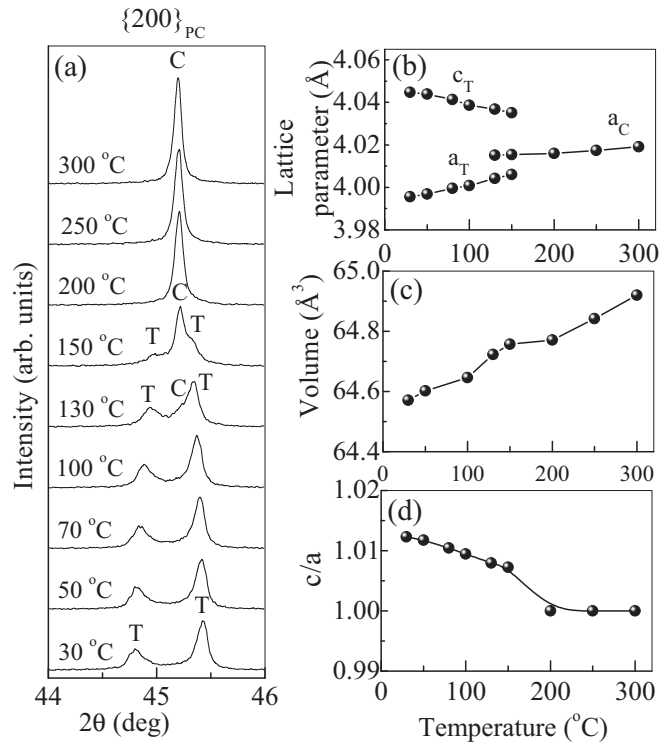

FIG. 8. (a) Evolution of the pseudocubic $\{200\}_{pc}$ XRD profile of poled PT-BNZ ($x = 0.41$) with temperature. Data were collected during the heating cycle. (b) Variation of lattice parameter, (c) unit-cell volume, and (d) tetragonality (c/a) of poled PT-BNZ ($x = 0.41$) with temperature.

has been tilted precisely to the [100] direction. Despite being inclined to the surface, the domain walls intersect at ~ 90, restricting their habit planes, based on the crystallography of a perovskite cell, to either {001} or {110}. The habit planes of non-180° walls in a tetragonal ferroelectric are constrained to occupy {110} planes but for a rhombohedral both {001} and {110} planes are allowed. In the [100] direction of a cubic unit cell, {001} planes are either perpendicular to or parallel with the sample surface. Since the domain walls are inclined but nonetheless intersect at 90°, we conclude that their habit planes are {110}, consistent with the tetragonal structure, resolved by XRD and Raman.

Figure 11(b) is a 001 reflection, two-beam dark-field image of a grain in an unpoled sample of $x = 0.42$ with the electron beam along a [100] direction of the perovskite cell (diffraction pattern inset). The image shows two different scale lengths of domain structure. There is evidence of a mesoscale lamella (20–30 nm, center), typical of domains close to a structural phase boundary and a perturbation in diffraction contrast on the right-hand side of the image which we attribute to a nanodomain structure ($\sim 5-10$ nm). A nanodomain structure is typical of a relaxorlike phase which gives rise to an average cubiclike structure in macroscopic diffraction techniques such as XRD. The mesoscale domains are highly mobile in the electron beam but in general appear inclined to the TEM sample surface and intersect at 90° (as illustrated in the image). Therefore, their habit planes are {110}, consistent with a tetragonal ferroelectric. We note that in such a fine scale domain structure, local stresses around dislocations and during beam heating can affect the habit planes of domain walls. Nonetheless, TEM evidence favors the conclusion that the local structure of the mesoscale lamella regions is tetragonal which coexists with a relaxorlike pseudocubic nanodomain phase. These conclusions are consistent with Raman, XRD, and electrical measurements.

IV. DISCUSSION

A. Non-MPB nature of PT-BNZ

The enhancement of the piezoelectric response of PT-BNZ for compositions exhibiting coexistence of tetragonal and CL phases (in the unpoled state) is analogous to the conventional MPB systems exhibiting piezoelectricity enhancement in the phase coexistence (tetragonal + rhombohedral/monoclinic) region. From this analogy, one may be tempted to argue that the CL phase could be akin to rhombohedral/monoclinic [6]. This view may also be emboldened by the fact that a related system $(1\text{-}x)PbTiO_3-(x)BiScO_3$ (PT-BS) shows clear evidence of rhombohedral distortion (the splitting of pseudocubic $\{111\}_{pc}$ Bragg profile into two) on the global scale on the BS excess side of the MPB region [5,21]. A recent neutron pair distribution function analysis of unpoled $(1-x)$PT-(x)BNZ by Datta *et al.* [53] revealed a gradual change in the local structure from tetragonal to non-tetragonal with increasing composition (x). By comparing their results with those reported earlier for rhombohedral/monoclinic compositions of the PT-BS system [54], the authors argued in favor of the presence of MPB in PT-BNZ. As our study reveals, better clarity on such issues can be obtained after analyzing the structural state of the poled specimen. In the case of genuine MPB systems such as PZT

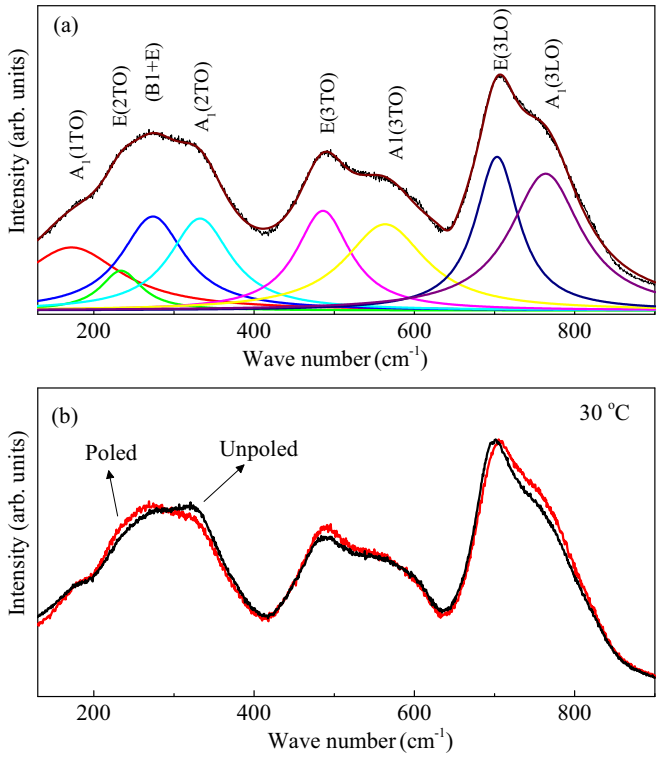

FIG. 9. (a) Lorentzian curve fitting of Raman peaks using tetragonal structure ($P4mm$) for PT-BNZ ($x = 0.41$). (b) Comparison of the Raman spectrum at room temperature (30 °C) for the poled and unpoled samples.

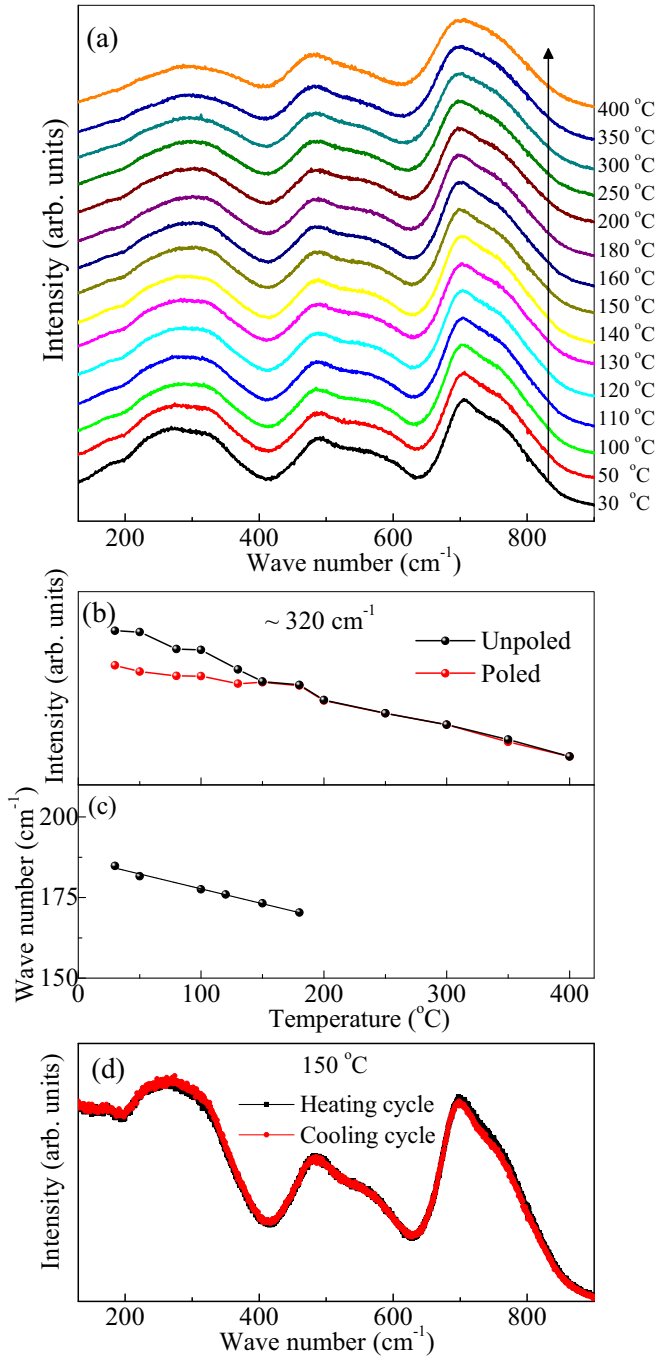

FIG. 10. (a) Evolution of the Raman spectrum (BE corrected) of poled PT-BNZ ($x = 0.41$) with temperature. (b) Temperature variation of the intensity of the Raman mode at ~320 cm^{-1} for poled and unpoled PT-BNZ ($x = 0.41$). (c) Temperature dependence of A_1(1TO) Raman mode ~180 cm^{-1}. (d) Comparison of the raw Raman spectrum (not corrected for BE factor) at 150 °C obtained during first heating and then cooling of the poled sample. The cooling data were collected after heating the specimen at 400 °C.

and PT-BS, poling merely changes the relative fraction of the coexisting phases [21,36]. It does not almost eliminate one of the coexisting phases as we see in our case (Fig. 5). The characteristic Raman modes of rhombohedral/monoclinic and tetragonal symmetries have also been identified in the Raman spectrum of the MPB composition of PZT [55], lending authenticity to their existence as a genuine structural phase on the local scale. This is not the case with PT-BNZ.

The qualitative difference between PT-BS and PT-BNZ from the structural standpoint can also be ascertained from the way the compositions exhibiting the dominant rhombohedral/monoclinic phase in the PT-BS system and the dominant CL phase in the PT-BNZ systems behave after poling. Lalitha *et al.* have shown that the PT-BS compositions with dominant rhombohedral/monoclinic phase do not show poling induced change in structure [5]. This contrasts with the fact that the equivalent composition in PT-BNZ exhibiting predominantly CL phase ($x = 0.44$) transforms to tetragonal after poling (Fig. 5). Our TEM examination clearly reveals that although the domains are highly miniaturized in the CL phase the tetragonal structure is still retained. The poling field increases the size of the tetragonal domains by increasing their coherence length. This appears as an irreversible CL→ $P4mm$ transformation in the XRD study. In this context, it is interesting to note that the local monoclinic deviations reported by Datta *et al.* [53] are slight departures from the [001] direction. This suggests that the decrease in the coherence length of the tetragonal regions (CL phase) is associated with the onset of positional disorder (departures from the [001] tetragonal distortion). If the CL phase of PT-BNZ were similar to the disordered monoclinic phase of PT-BS as argued in Ref. [53], we should expect both the systems to respond to the poling field in similar fashion. This, however, is not the case. While poling retains the average rhombohedral distortion in PT-BS [5], the CL phase of PT-BNZ ($x = 0.44$) is rather transformed to tetragonal after

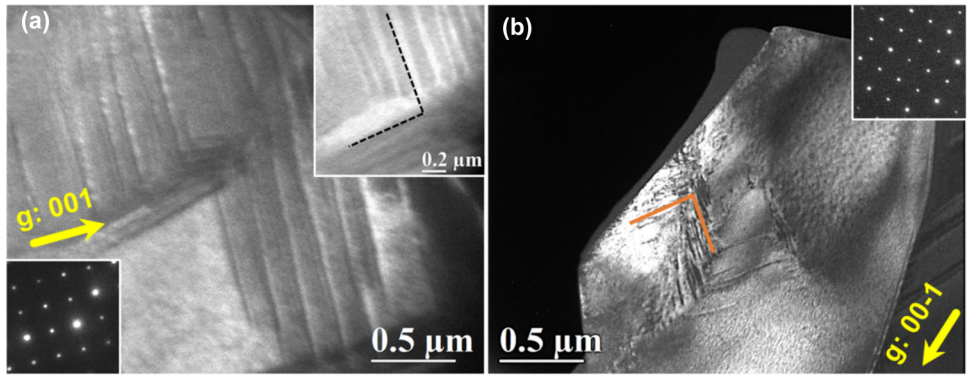

FIG. 11. (a) Dark-field TEM image from the poled $x = 0.42$ sample acquired close to [100] zone axis using $g = 001$. The bottom left-hand inset shows the selected area diffraction pattern (SAD) pattern acquired from the grain displayed in (a) and the top right-hand inset shows a region of the grain which has been tilted precisely to the [100] direction. (b) Dark-field TEM image from the unpoled $x = 0.42$ sample acquired along the [100] direction using $g = 00\bar{1}$. The top right-hand inset shows the SAD pattern acquired from the grain displayed in (b).

poling, Fig. 5. This confirms that the CL phase of PT-BNZ comprises tetragonal regions of small coherence length (and not rhombohedral regions of small coherence length). Thus, what appears as a two-phase ($P4mm + \text{CL}$) state on the global scale in PT-BNZ is actually a coexistence of short- and long-range tetragonal regions. A similar scenario has been reported earlier using pair distribution function analysis of the CL phase in $BaTiO_3$-$Bi(Zn_{1/2}Ti_{1/2})O_3$ [56] and more recently in a La-modified $BiFeO_3$-$PbTiO_3$ system showing extraordinarily large electrostrain [57]. Usher *et al.* have shown that the average structure of $BaTiO_3$-$Bi(Zn_{1/2}Ti_{1/2})O_3$ appears tetragonal on a smaller length scale and cubic on a larger length scale [56]. In this context, the decrease in the measured tetragonality with decreasing fraction of the tetragonal phase in the unpoled specimens [Fig. 2(b)], and the increase of tetragonality after poling [i.e., after suppression of the CL, Fig. 5(b)], can be associated to the correlation length of the tetragonal regions, and not a genuine increase in the tetragonality on the scale of unit cell.

B. Non-MPB and large electromechanical response

Our conclusion that the cubiclike phase is not rhombohedral/monoclinic, but tetragonal, has important implications. Polarization rotation [28] and the field induced interferroelectric transformations [36,37], which are often invoked to explain the enhanced piezoelectric response in conventional MPB systems (e.g., PZT), are no longer plausible mechanisms in PT-BNZ. The large electromechanical response of this system therefore appears to be associated with the miniaturization of the $P4mm$ domains and the ease of domain wall displacement [32–35]. The ease of domain wall motion is maximum for $x = 0.41$ as is evident from the minimum coercive field of this composition [Fig. 3(b)]. Recently, Narayan *et al.* reported a very large electrostrain (greater than 1%) in a similar system (La-modified $BiFeO_3$-$PbTiO_3$, BF-PT:La) [57]. This particular system is also non-MPB in nature. The electrostrain increases sharply when the random field due to La substitution starts miniaturizing the $P4mm$ domains, which manifests as the onset of a CL phase on the global scale [57]. The extraordinary electrostrain (>1%) in BF-PT:La is due to a combination of large tetragonality ($c/a \sim 2.2\%$), high mobility of the tetragonal domain walls as the CL phase sets in [57], and very large reverse switching of the tetragonal domains [58]. This discovery further confirms that polarization rotation and field induced interferroelectric transformation is not necessary for achieving large electromechanical response in piezoceramics.

C. Comparison with the cubiclike phase in $Na_{1/2}Bi_{1/2}TiO_3$-$BaTiO_3$

It is worth comparing the origin of the CL phase in PT-BNZ and that observed in the well-known lead-free piezoelectric $0.94Na_{1/2}Bi_{1/2}TiO_3$-$0.06BaTiO_3$ (NBT-6BT) [25,59,60]. The CL phase of NBT-6BT evolves from the monoclinic average structure of $Na_{1/2}Bi_{1/2}TiO_3$ (NBT) [61,62]. On poling NBT-6BT, the CL phase transforms to rhombohedral [60] or tetragonal + rhombohedral [25]. In contrast to $PbTiO_3$, which is a well-behaved classical ferroelectric, the parent compound NBT exhibits a high degree of positional disorder on the A site, and local in-phase octahedral tilt [63–68] which is incompatible with a long-range ferroelectric ($R3c$) order. The inherent positional disorder in NBT arises due to the qualitatively very different characteristics of the Na-O and Bi-O bonds [66]. Poling supresses the positional disorders [46,47,67], making the perceived monoclinic (Cc) structure transform irreversibly to rhombohedral ($R3c$) on the global scale. The onset of the CL phase in the unpoled state of NBT-6BT is a consequence of adding further disorder in the already (intrinsically) positionally disordered parent compound, NBT. This makes NBT-6BT a strong relaxor ferroelectric with significantly enhanced dielectric dispersion [68]. However, it is important to note that although both NBT-6BT and PT-BNZ exhibit CL phase, the piezoelectric response of the NBT-6BT is significantly low ($\sim$ 190 pC/N) as compared to PT-BNZ ($d_{33} \sim 400$ pC/N). Eerd *et al.* [69] have argued that the low d_{33} of NBT-6BT is because the system retains its local structural correlations even above the depolarization temperature, and that the depolarization is not associated with a thermodynamic instability. In contrast, our system does exhibit large piezoelectric ($d_{33} \sim 400$ pC/N) and electrostrain response ($\sim 0.5\%$

at 85 kV/cm) even though it also retains its local structure above the depolarization temperature. Both NBT-6BT and PT-BNZ being relaxors, the depolarization in both the systems is associated with the transformation of the system from the nonergodic to ergodic state. The local correlations are not expected to change dramatically in both cases.

D. Comparison of depolarization mechanisms in other systems

The fact that the system shows a weak dielectric anomaly at the depolarization temperature during the heating cycle of the poled specimen suggests that the depolarization, in spite of not being associated with a thermodynamic phase transition as in normal ferroelectrics, should be triggered by some kind of structural instability. A similar weak dielectric anomaly at $\sim 70\,^{\circ}$C, i.e., well below the dielectric maximum temperature (150 °C), has been reported during heating of a poled sample of the MPB composition of $PbTiO_3$-$Pb(Mg_{1/3}Nb_{2/3})O_3$ [70] and $(Ba,Ca)(Ti,Zr)O_3$ [71]. The anomalies in $PbTiO_3$-$Pb(Mg_{1/3}Nb_{2/3})O_3$ and $(Ba,Ca)(Ti,Zr)O_3$ have been attributed to temperature driven rhombohedral to tetragonal and orthorhombic-tetragonal interferroelectric structural transformation, respectively. The A_1(1TO) mode survives above the depolarization temperature in $PbTiO_3$-$Pb(Mg_{1/3}Nb_{2/3})O_3$ since the system is still in the ferroelectric phase of another symmetry (tetragonal) above the depolarization temperature. Hence although the temperature dependence of the dielectric behavior of poled specimens of conventional MPB systems (exhibiting coexistence of tetragonal and rhombohedral/monoclinic symmetries) and the non-MPB systems such as PT-BNZ, may mimic similar behavior, the mechanisms associated with the weak dielectric anomalies in the poled specimens in these systems are fundamentally different. In our case, (and perhaps in all such non-MPB systems) there is no visible sign of the change in structural symmetry across the depolarization temperature. The vanishing of the A_1(1TO) mode at the depolarization temperature is analogous to ferroelectric-paraelectric thermodynamic transformation. The dramatic loss of piezoelectricity on annealing the poled specimen system at the depolarization temperature is consistent with this observation. The piezoelectricity is not likely to decrease to such an extent if the depolarization is associated with an interferroelectric instability as in $PbTiO_3$-$Pb(Mg_{1/3}Nb_{2/3})O_3$ and $BaTiO_3$-based systems. In the case of NBT, Rao *et al.* [44] have demonstrated that the structural instability associated with depolarization is related to the onset of in-phase octahedral tilt—a structural distortion which is incompatible with long-range ferroelectric order and therefore breaks the long-range coherence in polarization induced by the poling field.

V. CONCLUSIONS

We have examined the crystal structure and domain structure of the compositions showing large electromechanical response in solid solutions of the ferroelectric system $PbTiO_3$-$Bi(Ni_{1/2}Zr_{1/2})O_3$ (PT-BNZ). The composition range which shows large piezoelectric response shows coexistence of tetragonal and CL phases in the unpoled state. The CL phase is suppressed for all the MPB compositions after poling. Examination of the domain structures revealed that the CL phase is associated with tetragonal-like domains of short coherence length. Poling increases the coherence length of the $P4mm$ regions, which manifests as a poling induced CL $\rightarrow$ $P4mm$ transformation on the global length scale (XRD). We also found a correspondence between the fraction of the $P4mm$ phase and the measured tetragonality. This suggests that the tetragonality perceived on the global scale (such as by XRD measurements) is a function of the correlation length of the tetragonal phase, which can as well be altered by the poling field. On heating, a lattice instability sets in well before the dielectric maximum temperature and destroys the larger coherence of tetragonal regions stabilized by the poling field. Our study confirms that the appearance of a two-phase ($P4mm$ + CL) state in PT-BNZ is not a consequence of interferroelectric instability which is the hallmark of conventional MPB/PPB systems. In the absence of a genuine interferroelectric instability, it is no longer possible to invoke field induced polarization rotation and/or interferroelectric transformation as plausible mechanisms to explain the large electromechancal response in PT-BNZ. The piezoelectric enhancement in the present case is associated with the inducement of structural heterogeneity via miniaturization of the ferroelectric-ferroelastic $P4mm$ domains, and does not involve a change of symmetry (even on the local scale). Based on our results, we argue that the ferroelectric solid solutions represented by the general formula $PbTiO_3$-$Bi(M'M'')O_3$ are promising systems for the design of non-MPB-based high-performance piezoelectric materials. These systems have the added advantage that they have significantly reduced Pb content and can serve as possible alternatives to conventional all-PB MPB alloys.

ACKNOWLEDGMENTS

R.P. gratefully acknowledges the Science and Engineering Research Board (SERB) of the Department of Science and Technology, Government of India, for financial support from the National Postdoctoral Fellowship (Grant No. PDF/2015/000169). R.R. gratefully acknowledges the SERB of the Ministry of Science and Technology, Government of India, for financial support (Grant No. EMR/2016/001457). I.M.R. and A.M. acknowledge the support of the United Kingdom Research and Innovation Grant No. EP/N032233/1.

[1] W. Liu and X. Ren, Phys. Rev. Lett. **103**, 257602 (2009).
[2] Y. Saito, H.Takao, T. Tani, T. Nonoyama, K.Takatori, T. Homma, T. Nagaya, and M. Nakamura, Nature **432**, 84 (2004).
[3] X. Wang, J. Wu, D. Xiao, J. Zhu, X. Cheng, T. Zheng, B. Zhang, X. Lou, and X. Wang, J. Am. Chem. Soc. **136**, 2905 (2014).
[4] R. E. Eitel, C. A. Randall, T. R. Shrout, P. W. Rehrig, W. Hackenberger, and S.-E. Park, Jpn. J. Appl. Phys. **40**, 5999 (2001).
[5] K. V. Lalitha, A. N. Fitch, and R. Ranjan, Phys. Rev. B **87**, 064106 (2013).

[6] Y. Rong, J. Chen, H. Kang, L. Liu, L. Fang, L. Fan, Z. Pan, and X. Xing, J. Am. Ceram. Soc. **96**, 1035 (2013).

[7] Z. Pan, J. Chen, L. L. Fan, L. J. Liu, L. Fang, and X. R. Xing, J. Appl. Phys. **112**, 114120 (2012).

[8] M. R. Suchomel, A. M. Fogg, M. Allix, H. Niu, J. B. Claridge, and M. J. Rosseinsky, Chem. Mater. **18**, 4987 (2006).

[9] A. A. Belik, T. Wuernisha, T. Kamiyama, K. Mori, M. Maie, T. Nagai, Y. Matsui, and E. T. Muromachi, Chem. Mater. **18**, 133 (2006).

[10] M. Azuma, K. Takata, T. Saito, S. Ishiwata, Y. Shimakawa, and M. Takano, J. Am. Chem. Soc. **127**, 8889 (2005).

[11] S. M. Choi, C. J. Stringer, T. R. Shrout, and C. A. Randall, J. Appl. Phys. **98**, 034108 (2005).

[12] C. A. Randall, R. Eitel, B. Jones, and T. R. Shrout, J. Appl. Phys. **95**, 3633 (2004).

[13] G. Shabbir, A. H. Qureshi, S. Kojima, and D. A. Hall, Ferroelectrics **346**, 72 (2007).

[14] M. R. Suchomel and P. K. Davies, Appl. Phys. Lett. **86**, 262905 (2005).

[15] D. M. Stein, M. R. Suchomel, and P. K. Davies, Appl. Phys. Lett. **89**, 132907 (2006).

[16] M. D. Snel, W. A. Groen, and G. de With, J. Eur. Ceram. Soc. **26**, 89 (2006).

[17] M. R. Suchomel and P. K. Davies, J. Appl. Phys. **96**, 4405 (2004).

[18] J. Chen, P. H. Hu, X. Y. Sun, C. Sun, and X. R. Xing, Appl. Phys. Lett. **91**, 171907 (2007).

[19] I. Grinberg and A. M. Rappe, Phys. Rev. Lett. **98**, 037603 (2007).

[20] S. Zhang, C. Stringer, R. Xia, S. M. Choi, C. A. Randall, and T. R. Shrout, J. Appl. Phys. **98**, 034103 (2005).

[21] K. V. Lalitha, A. K. Kalyani, and R. Ranjan, Phys. Rev. B **90**, 224107 (2014).

[22] B. Noheda, D. E. Cox, G. Shirane, J. A. Gonzalo, L. E. Cross, and S.-E. Park, Appl. Phys. Lett. **74**, 2059 (1999).

[23] A. K. Singh and D. Pandey, Phys. Rev. B **67**, 064102 (2003).

[24] R. Ranjan and A. Dviwedi, Solid State Commun. **135**, 394 (2005).

[25] R. Garg, B. N. Rao, A. Senyshyn, P. S. R. Krishna, and R. Ranjan, Phys. Rev. B **88**, 014103 (2013).

[26] I. P. Pronin, N. N. Parfenova, N. V. Zaitseva, V. A. Isupov, and G. A. Smolensky, Sov. Phys. Solid State **24**, 1060 (1982) [Fiz. Tverd. Tela **24**, 1860 (1982)].

[27] S.-E. Park and T. R. Shrout, J. Appl. Phys. **82**, 1804 (1997).

[28] H. Fu and R. E. Cohen, Nature **403**, 281 (2000).

[29] R. Guo, L. E. Cross, S.-E. Park, B. Noheda, D. E. Cox, and G. Shirane, Phys. Rev. Lett. **84**, 5423 (2000).

[30] D. Damjanovic, J. Am. Ceram. Soc. **88**, 2663 (2005).

[31] D. Damjanovic, Appl. Phys. Lett. **97**, 062906 (2010).

[32] D. Damjanovic and M. Demartin, J. Phys. D: Appl. Phys. **29**, 2057 (1996).

[33] Y. M. Jin, Y. U. Wang, A. G. Khachaturyan, J. F. Li, and D. Viehland, Phys. Rev. Lett. **91**, 197601 (2003).

[34] Y. M. Jin, Y. U. Wang, A. G. Khachaturyan, J. F. Li, and D. Viehland, J. Appl. Phys. **94**, 3629 (2003).

[35] J. L. Jones, E. Aksel, G. Tutuncu, T.-M. Usher, J. Chen, X. Xing, and A. J. Studer, Phys. Rev. B **86**, 024104 (2012).

[36] M. Hinterstein, J. Rouquette, J. Haines, Ph. Papet, M. Knapp, J. Glaum, and H. Fuess, Phys. Rev. Lett. **107**, 077602 (2011).

[37] M. Hinterstein, M. Hoelzel, J. Rouquette, J. Haines, J. Glaum, H. Kungle, and M. Hoffman, Acta Mater. **94**, 319 (2015).

[38] D. K. Khatua, K. V. Lalitha, C. M. Fancher, J. L. Jones, and R. Ranjan, Phys. Rev. B **93**, 104103 (2016).

[39] R.-J. Carvajal, FULLPROF 2000; A Rietveld Refinement and Pattern Matching Analysis Program, Laboratories Leon Brillouin (CEA-CNRS), France.

[40] B. Dkhil, J. M. Kiat, G. Calvarin, G. Bladinozzi, S. B. Vakhrushev, and E. Suard, Phys. Rev. B **65**, 024104 (2001).

[41] J.-M. Kiat, Y. Uesu, B. Dkhil, M. Matsuda, C. Malibert, and G. Calvarin, Phys. Rev. B **65**, 064106 (2002).

[42] A. M. Glazer, S. A. Mabud, and R. Clarke, Acta Cryst. B **34**, 1065 (1978).

[43] B. Noheda, J. A. Gonzalo, L. E. Cross, R. Guo, S.-E. Park, D. E. Cox, and G. Shirane, Phys. Rev. B **61**, 8687 (2000).

[44] B. N. Rao, R. Datta, S. S. Chandrashekaran, D. K. Mishra, V. Sathe, A. Senyshyn, and R. Ranjan, Phys. Rev. B **88**, 224103 (2013).

[45] Y.-H. Seo, J. Koruza, A. Bencan, B. Malic, J. Rodel, and K. G. Webber, J. Am. Ceram. Soc. **97**, 1582 (2014).

[46] B. N. Rao and R. Ranjan, Phys. Rev. B **86**, 134103 (2012).

[47] B. N. Rao, A. N. Fitch, and R. Ranjan, Phys. Rev. B **87**, 060102(R) (2013).

[48] G. A. Samara, J. Phys.: Condens. Matter **15**, R367 (2003).

[49] A. A. Bokov, M. Maglione, and Z. G. Ye, J. Phys.: Condens. Matter **19**, 092001 (2007).

[50] G. Burns and B. A. Scott, Phys. Rev. B **7**, 3088 (1973).

[51] J. D. Freire and R. S. Katiyar, Phys. Rev. B **37**, 2074 (1988).

[52] K. Datta, A. Richter, M. Gobbels, R. B. Neder, and B. Mihailova, Phys. Rev. B **92**, 024107 (2015).

[53] K. Datta, R. B. Neder, J. Chen, J. C. Neuefeind, and B. Mihailova, Phys. Rev. Lett. **119**, 207604 (2017).

[54] K. Datta, A. Richter, M. Göbbels, D. A. Keen, and R. B. Neder, Phys. Rev. B **93**, 064102 (2016).

[55] J. Frantti and V. Lantto, Phys. Rev. B **56**, 221 (1997).

[56] T.-M. Usher, T. Iamsasri, J. S. Forrester, N. Raengthon, N. Triamnak, D. P. Cann, and J. L. Jones, J. Appl. Phys. **120**, 184102 (2016).

[57] B. Narayan, J. S. Malhotra, R. Pandey, K. Yaddanapudi, P. Nukala, B. Dkhil, A. Senyshyn, and R. Ranjan, Nat. Mater. **17**, 427 (2018)

[58] X. Ren, Nat. Mater. **3**, 91 (2004).

[59] T. Li, X. Lou, X. Ke, S. Cheng, S. Mi, X. Wang, J. Shi, X. Liu, G. Dong, H. Fan, Y. Wang, and X. Tan, Acta Mater. **128**, 337 (2017).

[60] J. E. Daniels, W. Jo, J. Rodel, and J. L. Jones, Appl. Phys. Lett. **95**, 032904 (2009).

[61] S. Gorfman and P. A. Thomas, J. Appl. Crystallogr. **43**, 1409 (2010).

[62] E. Aksel, J. S. Forrester, J. L. Jones, P. A. Thomas, K. Page, and M. R. Suchomel, Appl. Phys. Lett. **98**, 152901 (2011).

[63] I. Levin and I. M. Reaney, Adv. Funct. Mater. **22**, 3445 (2012).

[64] J. Kreisel, P. Bouvier, B. Dkhil, P. A. Thomas, A. M. Glazer, T. R. Welberry, B. Chaabane, and M. Mezouar, Phys. Rev. B **68**, 014113 (2003).

[65] A. M. Balagurov, E. Y. Koroleva, A. A. Naberezhnov, V. P. Sakhnenko, B. N. Savenko, N. V. Ter-Oganessian, and S. B. Vakhrushev, Phase Trans. **79**, 163 (2006).

[66] V. A. Shuvaeva, D. Zekria, A. M. Glazer, Q. Zhang, S. M. Weber, P. Bhattacharya, and P. A. Thomas, Phys. Rev. B **71**, 174114 (2005)

[67] B. N. Rao, L. Olivi, V. Sathe, and R. Ranjan, Phys. Rev. B **93**, 024106 (2016).

[68] R. Garg, B. N. Rao, A. Senyshyn, and R. Ranjan, J. Appl. Phys. **114**, 234102 (2013).

[69] B. W. Eerd, D. Damjanovic, N. Klein, N. Setter, and J. Trodahl, Phys. Rev. B **82**, 104112 (2010).

[70] M. Shen, G. G. Siu, Z. K. Xu, and W. Cao, Appl. Phys. Lett. **86**, 252903 (2005).

[71] K. Brajesh, K. Tanwar, M. Abebe, and R. Ranjan, Phys. Rev. B **92**, 224112 (2015).